

# UC San Diego

## UC San Diego Previously Published Works

### Title

Effect of nearby piles and soil properties on thermal behaviour of a field-scale energy pile

### Permalink

<https://escholarship.org/uc/item/63k0z1n6>

### Journal

CANADIAN GEOTECHNICAL JOURNAL, 58(9)

### ISSN

0008-3674

### Authors

Moradshahi, Aria  
Faizal, Mohammed  
Bouazza, Abdelmalek  
[et al.](#)

### Publication Date

2021

### DOI

10.1139/cgj-2020-0353

Peer reviewed

## Effect of nearby piles and soil properties on the thermal behaviour of a field-scale energy pile

Journal:	<i>Canadian Geotechnical Journal</i>
Manuscript ID	cgj-2020-0353.R2
Manuscript Type:	Article
Date Submitted by the Author:	19-Oct-2020
Complete List of Authors:	Moradshahi, Aria; Monash University, Civil Engineering Faizal, Mohammed; Monash University, Civil Engineering Bouazza, Abdelmalek; Monash University, McCartney, John; University of California San Diego, Structural Engineering
Keyword:	Energy Piles, Thermal Interaction, Field tests
Is the invited manuscript for consideration in a Special Issue? :	Not applicable (regular submission)

SCHOLARONE™  
 Manuscripts

1 **Effect of nearby piles and soil properties on the thermal behaviour of a field-scale energy**  
2 **pile**

3

4 **Aria Moradshahi**

5 PhD student, Monash University, Department of Civil Engineering, 23 College Walk, Clayton,  
6 Vic. 3800, Australia. Telephone: +61 3 990 58901; Email: aria.moradshahi@monash.edu

7

8 **Mohammed Faizal**

9 Research Fellow, Monash University, Department of Civil Engineering, 23 College Walk,  
10 Clayton, Vic. 3800, Australia. Telephone: +61 3 9902 9988; Email:  
11 mohammed.faizal@monash.edu

12

13 **\* Abdelmalek Bouazza (Corresponding Author)**

14 Professor, Monash University, Department of Civil Engineering, 23 College Walk, Clayton,  
15 Vic. 3800, Australia. Telephone: +61 3 9905 4956; Email: malek.bouazza@monash.edu

16

17 **John S. McCartney**

18 Professor and Department Chair, University of California San Diego, Department of Structural  
19 Engineering, 9500 Gilman Drive, SME 442J, La Jolla, CA 92093-0085, USA, Telephone:  
20 +1 858 534 9630; Email: mccartney@ucsd.edu

21

22

23

24

25

26

27

**Abstract**

The thermal response of an energy field scale pile that is part of a pair of energy piles spaced at a centre-to-centre distance of 3.5 m (i.e. 6 D, where D is the pile diameter), was examined experimentally and numerically. Three field tests were conducted to assess the axial and radial thermal responses of the energy pile: (1) heating of the energy pile alone; (2) heating of both energy piles simultaneously, and (3) heating of the other energy pile while the considered energy pile was not heated. Good agreement was obtained between the experimental and numerical evaluations of the energy pile during the tests. A parametric study of the validated numerical model was performed for each of the three tests to understand the effects of varying soil thermal conductivity, thermal expansion coefficient, and elastic modulus on the thermal response of the considered energy pile. The numerical results confirmed the field results that radial thermal stresses in the energy piles were insignificant compared to axial thermal stresses. The impact of elastic modulus of the soil was more significant on the thermal stresses of the energy pile compared to the effects of soil thermal conductivity and thermal expansion coefficient. The thermal stresses of the considered energy pile were not significantly affected when both energy piles were heated simultaneously, even though ground temperature changes between the energy piles were more significant due to thermal interaction. Only minor thermal effects on the non-thermal pile were observed during heating of one of the energy piles for different soil properties.

47

**Keywords:** *Energy piles; thermal interaction; field tests;*

49

50

51

52

## 53 **Introduction**

54 Energy piles may interact with other energy piles or nearby standard piles through a  
55 coupled heat transfer and volume change in the surrounding soil. Although there have been  
56 several studies on energy pile groups using field testing and numerical simulations, the role of  
57 soil properties on this interaction is not well understood. For example, field studies conducted  
58 by Mimouni and Laloui (2015) showed that thermal interactions between thermal and non-  
59 thermal piles, for spacing ranging from 3 D to 5 D, could lead to the development of differential  
60 thermal loads in the piles. Field studies on a group of 6 energy piles conducted by You et al.  
61 (2014) indicated that ground temperatures overlapped between closely spaced (5 D) energy  
62 piles. However, the effect of this overlap on the thermal response of the piles was not  
63 investigated. Field tests on the axial thermal responses of a group of eight energy piles spaced  
64 between 9 m and 12 m (15 D and 20 D) were conducted by Murphy and McCartney (2014)  
65 and Murphy et al. (2015). The recorded ground temperatures indicated that the energy piles  
66 likely did not interact thermally during the duration of the thermal response tests. Rotta Loria  
67 and Laloui (2018) reported the results from field tests on thermal interaction between a  
68 triangular-spaced energy pile group with the same spacing as Mimouni and Laloui (2015) that  
69 included both operational and non-operational energy piles. They found that higher  
70 displacements and lower stresses occurred when all of the energy piles were heated. These  
71 observations were confirmed in full-scale tests on a row of energy piles, with 5 D spacing,  
72 performed by Wu et al. (2020).

73 Small-scale physical modelling (Peng et al. 2018; Wu et al. 2018) and numerical and  
74 analytical studies (Salciarini et al. 2015; Suryatriyastuti et al. 2016; Saggi and Chakraborty  
75 2016; Di Donna et al. 2016; Rotta Loria and Laloui 2016, 2017a, 2018) highlighted the  
76 presence of thermal interactions between energy piles. These studies also reported that the  
77 thermal stresses of individual energy piles might be affected up to 50% as a result of thermal

78 interaction with other piles. Most of these previous studies evaluated the axial thermal  
79 responses of energy piles, and only Mimouni and Laloui (2015) and Rotta Loria and Laloui  
80 (2017b) investigated the radial thermal reactions. A crucial gap in the current literature is that  
81 the previous studies did not assess the impact of varying some of the soil properties on the  
82 thermal responses of the piles. Some of these properties that could affect the thermal stresses  
83 in energy piles are the thermal conductivity,  $\lambda_{soil}$ , thermal expansion coefficient,  $\alpha_{soil}$ , and elastic  
84 modulus,  $E_{soil}$ , of the soil. Studies reported in current literature have investigated the effect of  
85 the soil above parameters for single energy piles; however, there is lack of knowledge on how  
86 these soil parameters can affect the energy pile thermal responses in case that more than one  
87 energy pile is operating.

88 For instance, the soil thermal conductivity,  $\lambda_{soil}$ , determines the magnitude of  
89 conductive heat transfer between the energy pile and the surrounding soils. Guo et al. (2018)  
90 and Salciarini et al. (2017) showed that soils with higher  $\lambda_{soil}$  tend to affect the temperature of  
91 a larger volume of soil surrounding an energy pile. An increase in  $\lambda_{soil}$  could, therefore, increase  
92 the thermal interaction between closely spaced energy piles. Previous numerical studies have  
93 indicated that soils with lower  $\lambda_{soil}$  tend to reduce the soil temperature changes due to more  
94 moderate heat transfer between the energy pile and the soil, hence leading to an increase in the  
95 energy pile temperature (Sani et al. 2019). Numerical studies also reported variations in axial  
96 thermal stresses of energy piles (Jeong et al. 2014; Salciarini et al. 2017) when  $\lambda_{soil}$  was varied.  
97 These studies indicate that  $\lambda_{soil}$  is a critical parameter that could affect the thermal responses of  
98 thermally interacting piles.

99 The soil thermal expansion coefficient,  $\alpha_{soil}$ , determines the magnitude of thermal  
100 deformations of the soil when subjected to temperature changes. The soil temperatures between  
101 thermally interacting energy piles are anticipated to be higher compared to isolated energy piles;  
102 thus, higher soil thermal deformations are also expected (You et al. 2014). The differences in

103 the thermal expansion coefficients of the pile concrete and the soil could affect the magnitudes  
104 of thermal stresses developed in the energy pile. This aspect has been highlighted by Rotta  
105 Loria and Laloui (2017b) in an experimental and numerical study on an energy pile surrounded  
106 by non-thermal piles. They indicated that the axial thermal stresses developed in the energy  
107 pile reduced when  $\alpha_{soil}$  was higher than that of the pile concrete. Similar observations were  
108 reported by Salciarini et al. (2017) for a single energy pile in a group of energy piles and by  
109 Bodas Freitas et al. (2013) and Bourne-Webb et al. (2015) on isolated energy piles. Further  
110 investigations on the impact of  $\alpha_{soil}$  will, therefore, provide more insight into the thermal  
111 responses of thermally interacting piles.

112 The elastic modulus of the soil,  $E_{soil}$ , may also affect the thermal responses of energy  
113 piles since the restraints to the pile thermal expansion/contraction is affected. A numerical  
114 study conducted by Khosravi et al. (2016) showed that an increase in  $E_{soil}$  led to the  
115 development of higher magnitudes of axial thermal stresses in an energy pile. Olgun et al.  
116 (2014) observed that increasing  $E_{soil}$  resulted in higher magnitudes of radial contact stresses at  
117 the pile-soil interface. These limited studies indicate that variation of  $E_{soil}$  could affect the axial  
118 and radial thermal responses of energy piles, and is, therefore, a subject of further investigation  
119 for thermally interacting piles.

120 This paper aims to examine the role of soil properties and nearby piles on the thermal  
121 behaviour of an energy pile. Field testing and numerical simulations were performed to  
122 understand the interaction between a pair of energy piles spaced at a centre-to-centre distance  
123 of 3.5 m (6 D). Three scenarios were investigated: (1) heating of the energy pile alone next to  
124 a non-operating energy pile; (2) heating of both energy piles simultaneously, and (3) heating  
125 of the other energy pile while the considered energy pile was not heated (i.e., a non-operating  
126 energy pile). After comparing the results from the experiments and field simulations for the  
127 three cases, a parametric evaluation was conducted to explore the effects of varying soil

128 properties (i.e. thermal conductivity,  $\lambda_{soil}$ , thermal expansion coefficient,  $\alpha_{soil}$ , and the elastic  
129 modulus,  $E_{soil}$ ) on the thermo-mechanical responses of one of the two energy piles.

130

### 131 **In-situ testing**

132

#### 133 ***Energy piles description and instrumentation***

134 The soil profile at the test site, summarized in Table 1, consisted of mostly dense sands  
135 and was part of the Brighton Group of materials described in detail in Barry-Macaulay et al.  
136 (2013) and Faizal et al. (2018; 2019a, 2019b). The site consisted of two cast-in-place bored  
137 energy piles with 0.6 m diameter and 10 m length located under a six-storey student residential  
138 building at a centre-to-centre distance of 3.5 m (Figure 1). The two energy piles were not linked  
139 with a pile-cap. Detailed information on the layout, installation and instrumentation of the  
140 energy piles is given in Faizal et al. (2019a). One of the two energy piles (EP1) was  
141 instrumented with axial and radial vibrating wire strain gauges and thermocouples. Whereas,  
142 the second energy pile (EP2) was only instrumented with three thermocouples on the external  
143 wall of the pipes. Four U-shaped heat exchanger loops made with high-density polyethylene  
144 (HDPE) pipes were attached to the reinforcing cages up to the depth of both piles. The inner  
145 and outer diameters of the HDPE pipes were 20 mm and 25 mm, respectively. The compressive  
146 strength and elasticity modulus of the unreinforced concrete measured in the laboratory were  
147 64 MPa and 34 GPa, respectively.

148 The considered energy pile (EP1) had vibrating wire strain gauges (VWSG) (Model:  
149 Geokon-4200) installed at five depths along the pile. There were five axial VWSGs (V1 to V5)  
150 and one radial VWSG (R) at each depth. The axial strain gauge V5 and radial strain gauge R  
151 were located near the centre of the pile while axial strain gauges V1 to V4 were located at  
152 approximately 160 mm away from the pile edge. Average magnitudes of temperatures, strains,



153 and stresses were considered from the axial VWSGs at a given depth. The water temperatures  
154 and flow rates at the inlet and outlet of the U-loops were recorded by Type T thermocouples  
155 and TM-series digital water flow meters, respectively. The ground temperatures were recorded  
156 using Type T thermocouples at two, 12 m deep, boreholes located between the two piles  
157 (Figure 1).

158

### 159 *Experimental procedure*

160 Three tests were conducted to investigate the aim of this study: (i) heating EP1 only,  
161 referred to as  $EP1_{active}$ , to establish the axial and radial thermal responses of EP1 (ii) heating  
162 EP1 and EP2 simultaneously, referred to as  $(EP1 + EP2)_{active}$ , to examine the effect of EP2 on  
163 the thermal response of EP1 (i.e. to investigate the impact of one operating energy pile on the  
164 other operating energy pile), and (iii) heating EP2 only, referred to as  $EP2_{active}$  to examine the  
165 effect of EP2 as an operating energy pile on the thermal response of EP1 as a nearby non-  
166 operating pile). The axial and radial thermal responses of EP1 were monitored in all the  
167 experiments due to its substantial instrumentation.

168 The ambient, inlet water and initial pile and ground temperatures for the three experiments  
169 are shown in Figure 2. The atmospheric temperatures used for all the parametric studies were  
170 obtained from a weather station located approximately 13 km from the experimental site  
171 (Figure 2a). The initial ground temperatures were measured by thermocouples located 0.63 m  
172 away from the edge of EP1 (Figure 1). The heating test on EP1 ( $EP1_{active}$ ) lasted for 18 days.  
173 Water at 48°C was circulated at a flow rate of 11 l/min in all the four loops. The experimental  
174 data for this experiment was reported in Faizal et al. (2019). The heating test on the two piles  
175 together,  $(EP1 + EP2)_{active}$ , lasted for 35 days. The piles were connected in series with a water  
176 flow rate of 11 L/min and temperature of 44°C. The heating test on EP2 ( $EP2_{active}$ ) lasted for  
177 40 days with a flow rate of 11 l/min and water temperature of about 46°C. The cases presented

178 herein are for continuous operation of ground source heat pumps that would be applicable to  
179 commercial buildings such as hospitals and any other application that require long term  
180 heating/cooling.

181

## 182 Numerical modelling

183 A numerical study was conducted to predict the thermal responses of EP1 for varying  
184 soil properties for all the three tests mentioned above. A three-dimensional finite element  
185 model was implemented in COMSOL Multiphysics software and was validated with the  
186 experimental results. A parametric evaluation of different  $\lambda_{soil}$ ,  $\alpha_{soil}$ , and  $E_{soil}$  was then  
187 conducted using the numerical model. The  $40 \times 15 \times 30$  m<sup>3</sup> 3D finite element model, shown in  
188 Figure 3, consisted of 344821 tetrahedral, triangular, prismatic, linear and vertex elements from  
189 which EP1 is described by 94273 mesh elements.

190 There was no groundwater encountered within the depth of the pile, and the soil at the site  
191 was considered to be dry. The energy piles and the soil were considered to be isotropic, porous  
192 media composed of solid particles with voids filled with air, and heat transfer was assumed to  
193 be purely conductive. The solid is considered to be incompressible under isothermal conditions.  
194 The inertial effects of the solid skeleton are negligible, and the simulations represent quasi-  
195 static conditions. The behaviour of all the materials is considered to be linear thermo-elastic,  
196 which is a reasonable assumption for relatively stiff soils like those encountered in the energy  
197 piles reported in the literature. The governing equations of the coupled thermo-mechanical  
198 problem commonly used in energy pile analysis are similar to those adopted by Caulk et al.  
199 (2014), Batini et al. (2015), Di Donna et al. (2016), and Rotta Loria and Laloui (2017b). The  
200 mechanical equilibrium equation can be written as follows:

$$201 \mathbf{F}_v = -\nabla \cdot \boldsymbol{\sigma} \quad (1)$$

202 where  $F_v$  is the volume force factor;  $\nabla$  indicates divergence; and  $\sigma$  is the total stress tensor. The  
 203 heat conduction equation can be written as follows:

$$204 \quad (\rho C)_{eff} \frac{\partial T}{\partial t} = -\nabla \cdot \lambda_{eff} \nabla T \quad (2)$$

205 where  $T$  is temperature and  $(\rho C)_{eff}$  and  $\lambda_{eff}$  are the effective volumetric heat capacity at  
 206 constant pressure and effective thermal conductivity, respectively. The thermal properties of  
 207 the fluid and solid materials were assumed to be temperature-dependent and temperature-  
 208 independent, respectively. To account for heat transfer in a porous media, the effective  
 209 volumetric heat capacity  $(\rho C)_{eff}$  and thermal conductivity  $\lambda_{eff}$  were considered as follows:

$$210 \quad (\rho C)_{eff} = \theta_p \rho_p C_{p,p} + (1 - \theta_p) \rho_s C_{p,s} \quad (3)$$

$$211 \quad \lambda_{eff} = \theta_p \lambda_p + (1 - \theta_p) \lambda_s \quad (4)$$

212 where  $(\rho C)_{eff}$  and  $\lambda_{eff}$  are the effective volumetric heat capacity at constant pressure and  
 213 effective thermal conductivity, respectively,  $\rho_p$  and  $\rho_s$  are pore fluid (air in this study) and soil  
 214 densities,  $\lambda_p$  and  $\lambda_s$  and  $C_{p,p}$  and  $C_{p,s}$  are representing thermal conductivities and specific heat  
 215 capacity of these two materials respectively.  $\theta_p$  is the volume fraction of solid material (the  
 216 ratio of the area occupied by the pore fluid to the entire cross-section of the soil).

217 Taking into account the thermal effects, Equation 1 can be rewritten as:

$$218 \quad \mathbf{F}_v = -\nabla \cdot (C_{ijkl} (\varepsilon_{ij} - \alpha \Delta T)) \quad (5)$$

219 where  $C_{ijkl}$  is the stiffness tensor, which is determined by material properties such as elastic  
 220 modulus and Poisson's ratio.  $\varepsilon_{ij}$  is the strain tensor,  $\alpha$  is the coefficient of thermal expansion,  
 221  $\Delta T$  is the change in temperature.

222 The energy conservation equation for water can be written as follows:

$$223 \quad \rho_f A C_f \frac{\partial T_f}{\partial t} + \rho_f A C_f u_f \cdot \nabla T_f = \nabla \cdot (A \lambda_f \nabla T_f) + Q_{wall} \quad (6)$$

224 where  $\rho_f$ ,  $C_f$ ,  $u_f$ ,  $\lambda_f$  and  $T_f$  are density, specific heat, velocity vector, thermal conductivity,  
 225 and temperature of the circulating fluid, respectively.  $A$  represents the cross-section of the pipe

226 in which fluid is flowing and  $Q_{wall}$  indicates the heat flux per unit length of the pipe and is  
 227 written as follows:

$$228 \quad Q_{wall} = h_{eff}(T_{ext} - T_f) \quad (7)$$

229 where  $h_{eff}$  is an effective pipe heat transfer coefficient considering the wetted perimeter of the  
 230 pipe cross-section; and  $T_{ext}$  is the external temperature surrounding the pipe. The effective heat  
 231 transfer coefficient for circular pipe shapes used in this study can be determined as follows:

$$h_{eff} = \frac{2\pi r_{int}}{\frac{1}{h_{int}} + \frac{r_{int}}{\lambda_p} \ln\left(\frac{r_{ext}}{r_{int}}\right)} \quad (8)$$

232 where  $r_{int}$  and  $r_{ext}$  are internal and external pipe radius, respectively;  $\lambda_p$  is pipe thermal  
 233 conductivity; and  $h_{int}$  is convective heat transfer coefficient inside the pipe which can be  
 234 obtained by:

$$h_{int} = \frac{Nu k_f}{d_h} \quad (9)$$

235 where  $d_h$  is the hydraulic diameter ( $d_h = \frac{4A}{2\pi r_{int}}$ ) and  $Nu$  is the Nusselt number for round pipes  
 236 and can be defined as a function of Reynolds,  $Re$ , and Prandtl,  $Pr$ , numbers, as follows:

$$237 \quad Nu = \max(3.66; Nu_{turb}) \quad (10.a)$$

$$Nu_{turb} = \frac{\left(\frac{f_D}{8}\right)(Re - 1000)Pr}{1 + 12.7 \sqrt{\frac{f_D}{8}} (Pr^{\frac{2}{3}} - 1)} \quad (10.b)$$

238

$$f_D = \left[ -1.8 \log\left(\frac{6.9}{Re}\right) \right]^{-1} \quad (10.c)$$

239 where  $f_D$  is the friction factor;  $Re = \rho_f V D / \mu$ ,  $Pr = \mu C_f / \lambda_f$ ,  $\rho_f$  is the fluid density,  $V$  is the  
240 velocity of the fluid,  $\mu$  is the dynamic viscosity of the fluid,  $D$  is pipe diameter,  $C_f$  and  $\lambda_f$  are  
241 the specific heat, and the thermal conductivity of the fluid, respectively.

242 The vertical boundaries at the sides of the model were assigned roller boundary  
243 conditions to allow vertical movement of the soil layers. A pinned boundary was applied at the  
244 base of the model, which prevents horizontal and vertical movements (Figure 3). The two  
245 energy piles and the soil were assumed to be bonded to each other at the pile-soil interface.  
246 Each energy pile is connected to a separate slab (with a dimension of  $5.0 \times 5.0 \times 0.5$  m) with  
247 perfect contact (full moment connection). The initial temperatures of the soil, pile, and the  
248 pipes were assumed to be the same as the initial ground temperatures recorded at the beginning  
249 of each experiment. A design downward concentrated axial load of 1400 kN similar to that of  
250 Faizal et al. (2019a,b) was applied at the surface of the slabs above the two pile heads to  
251 simulate the building loads. A diffusive surface was applied at the top boundary of the model  
252 to account for atmospheric temperature fluctuations which might affect the pile and soil  
253 temperatures for depths near the surface.

254 The soil, energy piles, slab and HDPE pipe properties used in the numerical model  
255 were selected based on previous studies conducted on the field site (Barry-Macaulay et al. 2013;  
256 Singh et al. 2015; Faizal et al. 2018, 2019a, 2019b) and from common properties reported in  
257 the literature (Bowles 1968; Mitchell and Soga 2005; Bourne-Webb et al. 2009; Amatya et al.  
258 2012). These properties are summarized in Table 1.

259

## 260 **Field results and numerical validation**

261 The field and numerical results are shown for average temperature changes of EP1,  
262  $\Delta T_{ave}$  of  $10^\circ\text{C}$  and  $20^\circ\text{C}$  for both  $EP1_{active}$  and  $(EP1 + EP2)_{active}$  tests (Figure 4). For  $EP1_{active}$ ,  
263 these temperature intervals correspond to 0.67, and 6 days of operation, respectively, and for

264 (EP1 + EP2)<sub>active</sub>, these intervals correspond to 6.2, and 13.9 days of operation, respectively.  
 265 For EP2<sub>active</sub>, the results are shown for the maximum temperature change of 2.2°C of EP1 as a  
 266 result of EP2 operation, corresponding to 40 days of operation.

267 The thermal strains,  $\varepsilon_T$ , were calculated as follows:

$$\varepsilon_T = (\varepsilon_i - \varepsilon_0)B + (T_i - T_0)\alpha_s$$

**(Error! No  
 text of  
 specified  
 style in  
 document.1)**

268 where  $\varepsilon_i$  is strain at the time  $i$ ,  $\varepsilon_0$  is the initial reference strain,  $B$  is the batch calibration  
 269 factor of the strain gauges with a value of 0.975,  $T_i$  is the temperature of the strain gauges at  
 270 time  $i$ ,  $T_0$  is the reference temperature of the strain gauges,  $\alpha_s$  is the coefficient of linear thermal  
 271 expansion of steel wire in the strain gauges (12.2  $\mu\text{ε}/^\circ\text{C}$ ).

272 The numerical axial and radial contact thermal stresses of EP1 were extracted from the  
 273 finite element analysis at the pile centre and the pile-soil interface, respectively. The  
 274 experimental axial thermal stresses in EP1 were estimated by the following equation:

$$275 \sigma_T = E_p(\varepsilon_{obs} - \alpha_{free}\Delta T) \quad (12)$$

276 where  $E_p$  is the elastic modulus of the concrete (taken as 34 GPa),  $\varepsilon_{obs}$  is experimentally  
 277 observed thermal strains,  $\alpha_{free}$  is the free thermal expansion coefficient of the concrete, taken  
 278 as 13  $\mu\text{ε}/^\circ\text{C}$  (Faizal et al., 2019a,b), and  $\Delta T$  is the change in temperature of the pile. The thermal  
 279 expansion coefficient of concrete selected in the current study is within the range of 9  $\mu\text{ε}/^\circ\text{C}$  to  
 280 14.5  $\mu\text{ε}/^\circ\text{C}$  reported by Stewart and McCartney (2014) and Bourne-Webb et al. (2016).

281 The experimental radial contact stresses of EP1 were estimated using cavity expansion  
 282 analysis as follows:

$$\sigma_n = \frac{E_s \Delta r}{(1 + \nu_s) r} \quad (13)$$

283 where  $E_s$  and  $\nu_s$  are the elastic modulus and Poisson's ratio of the surrounding dense sand,  
 284 respectively, assumed to be 60 MPa and 0.3, respectively, based on typical values for dense  
 285 sand (Faizal et al., 2019a,b; Elzeiny et al., 2020),  $r$  is the radius of EP1, and  $\Delta r$  is the thermally  
 286 induced radial displacement of EP1.

287 The field and numerical results of temperatures, and axial and radial thermal  
 288 strains/stresses of EP1 plotted against depth, for all experiments, are shown in Figure 4.  
 289 Positive thermal strains indicate expansion and negative thermal stresses indicate compression.  
 290 The numerical simulation results matched well with the in-situ results.

291 The temperatures of EP1 for EP1<sub>active</sub> and (EP1 + EP2)<sub>active</sub> tests (shown in Figures 4a  
 292 and 4b, respectively) were uniform with depth and reached a magnitude of approximately 38°C  
 293 for both cases. There were negligible differences in the temperatures for EP1 for all tests,  
 294 indicating that the operation of EP2 has insignificant effects on temperature of EP1 for the  
 295 given spacing of 3.5 m. The temperature change of EP1 is not significant in the EP2<sub>active</sub> test  
 296 compared to the EP1<sub>active</sub> and (EP1 + EP2)<sub>active</sub> tests and is also slightly non-uniform with depth,  
 297 possibly due to some atmospheric effects near the surface. The radial and axial thermal strains  
 298 (Figures 4c and 4d, respectively) and thermal stresses (Figures 4e and 4f) of EP1 increased  
 299 when  $\Delta T_{ave}$  increased from 10°C to 20°C for both EP1<sub>active</sub> and (EP1 + EP2)<sub>active</sub> tests. Due to  
 300 the slight increase in temperature of EP1 in the EP2<sub>active</sub> test, small variations in axial and radial  
 301 thermal strains/stresses were also observed in EP1. The lowest magnitude of axial thermal  
 302 strains (Figure 4d), and thus the highest axial thermal stresses (Figure 4f), were observed at a  
 303 depth of around 3 m in EP1 for all three experiments. This depth can be considered as the  
 304 location of the null point, indicating dominant stiffness of the overlying structure relative to  
 305 the stiffness imposed by the soil beneath the pile toe. The radial thermal strains of EP1 (Figure  
 306 4c) were significantly higher than the axial thermal strains of EP1 (Figure 4d) during the

307 EP1<sub>active</sub> and (EP1 + EP2)<sub>active</sub> tests, indicating the energy pile had less restraint to thermal  
308 expansion in the radial direction than in the axial direction. As a result, the radial thermal  
309 stresses (Figure 4e) were significantly lower than axial thermal stresses (Figure 4f) in EP1 for  
310 both EP1<sub>active</sub> and (EP1 + EP2)<sub>active</sub> tests.

311 Figure 5a shows the experimental and numerical change in ground temperatures with  
312 depth for EP1<sub>active</sub> and (EP1 + EP2)<sub>active</sub> tests at the two boreholes located at 0.63 m and 1.95 m  
313 from the edge of EP1 (Figure 1). The ground temperatures at depths of 7.28, 9.5, and 12 m were  
314 not recorded from day 7 of the EP2<sub>active</sub> experiment due to technical issues so the temperature data  
315 of this experiment was not shown in Figure 5a. The transient ground temperature changes with  
316 increasing radial distance from the sides of EP1 and EP2 for a depth of 5 m is shown in Figure  
317 5b. These ground temperatures are for  $\Delta T_{ave} = 20^{\circ}\text{C}$  of EP1 for EP1<sub>active</sub> and (EP1 + EP2)<sub>active</sub>  
318 tests and  $\Delta T_{ave} = 32^{\circ}\text{C}$  of EP2 in the EP2<sub>active</sub> test. The ground temperatures at a radial distance  
319 of 0 m and 2.9 m from the edge of EP1 are the soil-pile interface temperatures of EP1 and EP2,  
320 respectively (Figure 5b). The soil temperature changes between the piles are more significant  
321 for the (EP1 + EP2)<sub>active</sub> test, indicating that heating both piles simultaneously increased the  
322 thermal interaction between the piles due to overlapping of ground temperatures. The ground  
323 temperature change at the edge of EP2 is lower than at the edge of EP1 in the (EP1+EP2)<sub>active</sub>  
324 test. This is because the heat exchangers of the two piles were connected in series. Since EP1  
325 was heated first, the rate of heating of EP1 was higher than EP2, and the temperature of the  
326 fluid entering EP2 was lower than that entering EP1. As a result, EP1 had higher temperature  
327 changes than EP2, which resulted in lower temperatures at the edge of EP2. The ground  
328 temperatures predicted by numerical simulations matched well with the field results.

329

### 330 Numerical investigation



331 A parametric evaluation using the validated numerical model was conducted to  
332 investigate the effect of soil elastic modulus,  $E_{soil}$ , thermal expansion coefficient,  $\alpha_{soil}$ , and  
333 thermal conductivity,  $\lambda_{soil}$ , on the thermal responses of EP1 for the three field tests described  
334 above. Three different values of each soil parameter were considered for all soil layers typical  
335 of sandy soil profiles after Bowles (1968) and Mitchel and Soga (2005) (i.e.  $0.5E_{soil}$ ,  $E_{soil}$ ,  $2E_{soil}$ ;  
336  $0.5\lambda_{soil}$ ,  $\lambda_{soil}$ ,  $2\lambda_{soil}$ ; and  $0.1\alpha_{soil}$ ,  $\alpha_{soil}$ ,  $10\alpha_{soil}$ ). The parameters of  $E_{soil}$ ,  $\lambda_{soil}$ , and  $\alpha_{soil}$  have the same  
337 magnitudes used for the numerical validation of experimental results (Table 1).

338 The experimental data for all three field tests had different inlet fluid temperatures,  
339 different atmospheric temperatures and different initial pile and ground temperatures (Figure  
340 2). In the parametric study, however, the same test and boundary conditions were applied to all  
341 three simulations to assess better the effects of individual soil properties under the same  
342 boundary conditions, i.e. same inlet fluid temperatures, fluid velocity (11 L/min), initial pile  
343 and ground temperatures, and ambient temperatures. The ambient, inlet fluid and initial pile  
344 and ground temperatures used in the parametric study are obtained from EP1<sub>active</sub> test (Figure  
345 2) and are shown in Figure 6. The inlet fluid temperatures represent typical fluid temperatures  
346 for energy piles during heating mode of a GSHP.

347 The parametric simulations were conducted for 14 days for all three field tests. The  
348 results in the following sections are presented at Day 14 of the tests. In the parametric  
349 evaluation, it was assumed that the two energy piles were working separately (not connected  
350 in series) with the same inlet fluid temperatures, as shown in Figure 6b. This was done so that  
351 both energy piles had the same inlet fluid temperatures when heated simultaneously. Heating  
352 the two piles together in series would reduce the inlet fluid temperatures to EP2 compared to  
353 that of EP1 since EP1 will have a faster rate of heating, as was observed in the field test.

354

### 355 ***Pile and ground temperatures***

356           The effect of varying soil properties on the change in pile temperatures of EP1 and  
357 change in ground temperatures between the two piles is shown in Figure 7a and Figure 7b,  
358 respectively. The pile temperatures and ground temperatures were not affected by variations in  
359  $E_{soil}$  and  $\alpha_{soil}$  for all three tests (not shown here). The temperatures of EP1 reduced by  
360 approximately 2.5°C when  $\lambda_{soil}$  increased from  $0.5\lambda_{soil}$  to  $2\lambda_{soil}$  (Figure 7a) for both EP1<sub>active</sub> and  
361 (EP1+EP2)<sub>active</sub> tests. Higher values of  $\lambda_{soil}$  caused faster heat propagation in the soil, which  
362 resulted in lower thermal confinement around EP1, hence lower pile temperatures of EP1 are  
363 observed. For a given  $\lambda_{soil}$ , the temperatures of EP1 were same for both EP1<sub>active</sub> and  
364 (EP1+EP2)<sub>active</sub> tests since the operation of EP2 did not affect the soil temperature at the edge  
365 of EP1, even though higher ground temperature changes occurred between the piles when both  
366 piles were heated simultaneously, as shown in Figure 7b. No significant changes were observed  
367 in temperatures of EP1 for the EP2<sub>active</sub> test. Negative temperature changes of EP1 near the  
368 surface during the EP2<sub>active</sub> test is due to the very low atmospheric temperatures at Day 14  
369 (Figure 6a).

370           The ground temperatures during the EP1<sub>active</sub> test reduced with increasing radial  
371 distance from the edge of EP1. The ground temperatures during the (EP1+EP2)<sub>active</sub> test also  
372 initially reduced with increasing radial distance from the edges of EP1 and EP2, but eventually  
373 overlapped and developed higher temperatures near the mid-point between the two energy piles.  
374 This overlapping of ground temperatures indicates the presence of thermal interaction between  
375 the two energy piles when heated simultaneously in the (EP1+EP2)<sub>active</sub> test.

376           Increasing  $\lambda_{soil}$  reduced the ground temperatures near the energy piles, confirming the  
377 findings of Salciarini et al. (2017). This occurred due to higher heat propagation away from the  
378 energy piles when  $\lambda_{soil}$  was increased. As a result of faster heat propagation near the piles, the  
379 ground temperatures increased farther away from the piles for both EP1<sub>active</sub> and  
380 (EP1+EP2)<sub>active</sub> tests.

381

382 ***Pile axial thermal strains and stresses***

383 The effect of varying soil properties on the axial thermal strains and stresses of EP1 for  
384 all three test conditions are shown in Figure 8. The location of the maximum thermal stresses  
385 in EP1 remained approximately at the same depth of 3 m for all studied cases. Varying  $E_{soil}$  had  
386 more effects on the axial thermal strains and stresses of EP1 compared to the impacts of  $\lambda_{soil}$   
387 and  $\alpha_{soil}$  for all three field tests.

388 The effects of  $E_{soil}$  on the axial thermal strains and stresses of EP1 are shown in Figure  
389 8a and Figure 8b, respectively. An increase in  $E_{soil}$  significantly increased the axial thermal  
390 stresses in EP1 for both EP1<sub>active</sub> and (EP1+EP2)<sub>active</sub> tests. Similar observations were noted by  
391 Khosravi et al. (2016). The axial thermal stresses in EP1 almost doubled in EP1<sub>active</sub> and  
392 (EP1+EP2)<sub>active</sub> tests at 3 m depth when  $E_{soil}$  increased from  $0.5E_{soil}$  to  $2E_{soil}$ . Higher  $E_{soil}$  results  
393 in higher rigidity of the soil; hence, a higher restriction is imposed on the axial thermal  
394 expansion of the energy pile (Figure 8a). For a given  $E_{soil}$ , the thermal stresses developed in  
395 EP1 were similar for the EP1<sub>active</sub> and (EP1+EP2)<sub>active</sub> tests, with slight differences in the upper  
396 section of the pile. This indicates that the operation of one energy pile did not affect the thermal  
397 stresses developed in the nearby operating energy pile when both piles were heated  
398 simultaneously. Operation of EP2 in the EP2<sub>active</sub> test induced insignificant thermal axial strains  
399 and stresses in EP1, indicating that the heating of an energy pile had negligible effects on the  
400 nearby non-operating pile. This can be due to the fact that EP1 and EP2 are not connected by  
401 a pile-cap. The slightly positive (tensile) axial thermal stresses developed in the upper parts of  
402 EP1 in the EP2<sub>active</sub> test (Figure 8b) can be attributed to negative temperature changes in EP1  
403 due to atmospheric effect (see Figure 7a).

404 Figure 8c and 8d show the effects of  $\lambda_{soil}$  on the axial thermal strains and stresses of  
405 EP1, respectively. The thermal stresses developed in EP1 were lower than those developed for

406 different  $E_{soil}$ . There was a slight increase in axial thermal stresses of EP1 when  $\lambda_{soil}$  was  
407 increased from  $0.5\lambda_{soil}$  to  $2\lambda_{soil}$  in EP1<sub>active</sub> and (EP1+EP2)<sub>active</sub> tests (by approximately 0.3 MPa  
408 at 3 m depth), even though the pile temperatures had reduced by 2.5°C (Figure 7a). This could  
409 be attributed to the lower expansion of the soil near the pile-soil interface as a result of lower  
410 ground temperatures for larger thermal conductivity (Figure 7) which possibly increased  
411 restraint of the axial thermal expansion of the pile. The thermal strains and stresses in EP1 were  
412 similar for both EP1<sub>active</sub> and (EP1+EP2)<sub>active</sub> for any given  $\lambda_{soil}$  with slight differences in the  
413 upper pile section, indicating negligible thermal effects of one energy pile on the other when  
414 heated simultaneously. The magnitudes of axial thermal stresses and strains in EP1 in the  
415 EP2<sub>active</sub> test were negligible indicating negligible thermal effects on a nearby non-thermal pile  
416 due to the operation of an energy pile.

417 The effects of  $\alpha_{soil}$  on the axial thermal strains and stresses of EP1, are shown in Figures  
418 8e and 8f, respectively. The range of thermal stresses was lower than that for  $E_{soil}$ . Similar to  
419 what was observed for  $E_{soil}$  and  $\lambda_{soil}$ , the thermal stresses in EP1 were similar for both EP1<sub>active</sub>  
420 and (EP1+EP2)<sub>active</sub> test with slight differences in the upper pile section, for a given  $\alpha_{soil}$ .  
421 Increasing  $\alpha_{soil}$  to  $10\alpha_{soil}$  (corresponding to  $\alpha_{soil}/\alpha_{pile}$  of 0.7 and 7 respectively) resulted in a  
422 small reduction in axial thermal stresses in EP1 for both EP1<sub>active</sub> and (EP1+EP2)<sub>active</sub> tests,  
423 mostly for the upper pile section for  $10\alpha_{soil}$  ( $\alpha_{soil}/\alpha_{pile}$  of 7). This can be related to the increased  
424 soil expansion for higher values of  $\alpha_{soil}$  which resulted in a lower restriction on EP1. This  
425 behaviour is consistent with the observations reported by Bourne-Webb et al. (2016) and  
426 Salciarini (2017). Similar to the effects of  $E_{soil}$  and  $\lambda_{soil}$ , there were negligible effects of EP2  
427 operation on EP1 in the EP2<sub>active</sub> test. The values of  $\alpha_{soil}/\alpha_{pile}$  used in this study are consistent  
428 with those of other studies which have been reported to vary between 0 and 2 (Bodas Freitas  
429 et al., 2013), 0.033 and 3.3 (Rotta Loria and Laloui 2017), and 1 to 10 (Salciarini et al. 2017).  
430

### 431 *Pile radial thermal strains and stresses*

432 The effects of varying soil properties on the radial thermal strains and stresses of EP1  
433 for the three test scenarios are shown in Figure 9. The magnitudes of the radial thermal stresses  
434 in EP1 for all investigated soil parameters were significantly lower than the axial thermal  
435 stresses shown in Figure 8. The radial thermal strains were more significant and closer to the  
436 free thermal expansion of the pile compared to the axial thermal strains reported in Figure 8.  
437 These confirm the findings of previous studies that radial thermal stresses are insignificant  
438 compared to the magnitudes of axial thermal stresses in energy piles (Ozudogru et al. 2015;  
439 Gawecka et al. 2017; Faizal et al. 2018, 2019). The highest magnitudes of radial thermal  
440 stresses in EP1 for all cases are at a depth of 3 m due to the higher soil rigidity at this depth.  
441 Also,  $E_{soil}$  had higher impacts on the radial thermal stresses in EP1 compared to  $\lambda_{soil}$  and  $\alpha_{soil}$ .

442 The effect of  $E_{soil}$  on the radial thermal strains and stresses of EP1 are shown in Figures  
443 9a and 9b, respectively. An increase in  $E_{soil}$  resulted in an increase in the magnitudes of radial  
444 thermal stresses in EP1 in EP1<sub>active</sub> and (EP1+EP2)<sub>active</sub> tests due to increased soil rigidity.  
445 These observations are consistent with the results reported by Olgun et al. (2014), where the  
446 normal stresses increased from 3.5 to 14 kPa when  $E_{soil}$  increased from 25 MPa to 100 MPa.  
447 For a given  $E_{soil}$ , the radial thermal stresses in EP1 were similar for EP1<sub>active</sub> and (EP1+EP2)<sub>active</sub>  
448 tests, with minor differences of approximately 5 kPa for  $2E_{soil}$ . This confirms the negligible  
449 effects of the operation of one energy pile on the other nearby energy pile for the setting  
450 investigated in this study. Insignificant stress changes of up to 2.2 kPa were observed in EP1  
451 during the EP2<sub>active</sub> test.

452 The effect of  $\lambda_{soil}$  on radial thermal strains and stresses of EP1 are shown in Figures 9c  
453 and 9d, respectively. The radial thermal stresses of EP1 slightly reduced when  $\lambda_{soil}$  increased,  
454 with a maximum reduction of 4.5 kPa at 3 m depth when  $\lambda_{soil}$  increased from  $0.5\lambda_{soil}$  to  $2\lambda_{soil}$ .  
455 No significant differences were observed in radial thermal stresses of EP1 between the EP1<sub>active</sub>

456 and  $(EP1+EP2)_{active}$  tests indicating insignificant thermal effects of the operation of one energy  
457 pile on the other energy pile. Similar to  $E_{soil}$ , negligible stress changes of up to 2.2 kPa were  
458 observed in EP1 in the  $EP2_{active}$  test.

459 The effects of  $\alpha_{soil}$  on the radial thermal strains and stresses in EP1, are shown in Figures  
460 9e and 9f, respectively. The radial thermal stresses in EP1 increased for both  $EP1_{active}$  and  
461  $(EP1+EP2)_{active}$  tests with increasing  $\alpha_{soil}$ . The radial thermal stresses in EP1 in the  $EP1_{active}$   
462 test were higher than in the  $(EP1+EP2)_{active}$  test for  $0.1\alpha_{soil}$  and  $\alpha_{soil}$  (corresponding to  $\alpha_{soil}/\alpha_{pile}$   
463 of 0.07 and 0.7 respectively). However, for  $10\alpha_{soil}$  ( $\alpha_{soil}/\alpha_{pile}$  of 7) the opposite behaviour is  
464 observed due likely to increased thermal expansion of the soil. A higher volume of soil is  
465 subjected to temperature change when both piles are heated together (Rotta Loria and Laloui  
466 2017b). The radial thermal stresses in EP1 during the  $EP2_{active}$  test was very low compared to  
467 the  $EP1_{active}$  and  $(EP1+EP2)_{active}$  tests.

### 469 ***Thermal displacements***

470 The effects of varying soil properties on the axial and radial thermal displacements of  
471 EP1, for all three test scenarios, is shown in Figure 10. The radial thermal displacements were  
472 very low with a range of -0.03 mm to 0.01 mm, for all soil properties. The axial thermal  
473 displacements at the pile head of EP1 were much higher than radial thermal displacements and  
474 ranged between 0.3 mm to 0.5 mm for all soil properties. The radial and axial thermal  
475 displacements of EP1 were, however, up to 0.005% and 0.1% of the pile diameter, respectively,  
476 much lower than the generally allowable 10% of the pile diameter failure criteria.

477 Increasing  $E_{soil}$  resulted in a slight decrease in axial thermal displacements of EP1 for  
478 both  $EP1_{active}$  and  $(EP1+EP2)_{active}$  tests due to the higher restriction of the surrounding soil  
479 (Figure 11b). The axial thermal displacements of EP1 also reduced with increasing  $\lambda_{soil}$  for both  
480  $EP1_{active}$  and  $(EP1+EP2)_{active}$  tests, likely due to increased soil strength near the pile due to

481 temperature changes. Increasing  $\alpha_{soil}$  did not significantly affect the axial thermal displacement  
482 of EP1 for both  $EP1_{active}$  and  $(EP1+EP2)_{active}$  tests. There were no significant differences in  
483 axial and radial thermal displacements of EP1 between the  $EP1_{active}$  and  $(EP1+EP2)_{active}$  tests  
484 for all soil properties, confirming the negligible effects of the operation of one energy pile on  
485 the other. The axial and radial thermal displacements of EP1 for the  $EP2_{active}$  test were  
486 insignificant for all soil properties confirming negligible effects of an operating energy pile on  
487 a nearby non-thermal pile

#### 488 **Concluding remarks**

489 This paper examined the thermal responses of one of a pair of field-scale energy piles  
490 spaced at a centre-to-centre distance of 3.5 m. A parametric study was conducted with a  
491 numerical model validated with field tests to explore the effects of varying soil thermal  
492 conductivity, thermal expansion coefficient, and elastic modulus on the thermal response of  
493 the considered energy pile. Heating the two piles together increased thermal interaction  
494 between the piles due to higher ground temperature changes between the piles due to thermal  
495 overlapping. This thermal interaction, however, did not affect the magnitude of thermal stresses  
496 developed in the considered energy pile for all soil properties, indicating negligible thermal  
497 effects from the operation of one energy pile on the other energy pile during simultaneous  
498 heating. Heating only one pile also induced insignificant thermal effects on the other non-  
499 thermal pile for all soil properties. This outcome indicates that the operation of energy piles  
500 will not induce thermal stresses in nearby non-operating piles in the setting investigated in this  
501 paper. The effect of elastic modulus of the soil was more significant on the thermal stresses  
502 and displacements developed in the considered energy pile compared to the impact of thermal  
503 conductivity and thermal expansion coefficient of the soil. Increasing thermal conductivity of  
504 the soil, however, induced higher ground temperature changes around both energy piles. The  
505 numerical simulations confirmed the field results that the magnitudes of radial thermal stresses

506 developed energy piles were insignificant compared to the axial thermal stresses for all soil  
507 properties. The thermal displacements of the considered energy pile were negligible and  
508 significantly lower than 10% of the pile diameter for all studied cases and are not expected to  
509 affect the structural integrity of the energy piles. The results of this paper will be useful in  
510 assessing the thermal interaction among closely spaced energy piles that are not linked by a  
511 pile-cap when designing energy piles at different sites with soil properties similar to those  
512 reported in this paper. It should be noted that for energy piles spaced closer to each other (i.e.,  
513 in secant or tangent walls), thermal interaction between the energy piles might be more  
514 significant.

515

#### 516 **Acknowledgements**

517 This research project was supported under the Australian Research  
518 Council's Linkage Projects funding scheme (project number LP120200613). The authors also  
519 acknowledge the Australian Government Research Training Program Scholarship provided to  
520 the first author. The US National Science Foundation grant CMMI-0928159 supported the  
521 fourth author. The support of all the sponsors (Geotechnical Engineering-Acciona, Golder  
522 Associates, Geoexchange Australia, Brookfield-Multiplex) is gratefully acknowledged.

523

#### 524 **References**

- 525 Abdelaziz, S.L., and Ozudogru, T.Y. 2016. Selection of the design temperature change for  
526 energy piles. *Applied Thermal Engineering*, **107**: 1036-1045.  
527 <https://doi.org/10.1016/j.applthermaleng.2016.07.067>.
- 528 Akrouch, G., Sánchez, M., and Briaud, J-L. 2014. Thermo-mechanical behavior of energy piles  
529 in high plasticity clays. *Acta Geotechnica*, **9**(3): 399-412.  
530 <https://doi.org/10.1007/s11440-014-0312-5>.



- 531 Amatya, B.L., Soga K., Bourne-Webb P.J. 2012. Thermo-mechanical behaviour of energy piles.  
532 *Géotechnique*, **62**(6):503-519. <https://doi.org/10.1680/geot.10.P.116>.
- 533 Barry-Macaulay, D., Bouazza, A., Singh, R., Wang, B., and Ranjith, P. 2013. Thermal  
534 conductivity of soils and rocks from the Melbourne (Australia) region. *Engineering  
535 Geology*, **164**: 131-138. <https://doi.org/10.1016/j.enggeo.2013.06.014>.
- 536 Batini, N., Rotta Loria, A.F., Conti, P., Testi, D., Grassi, W. and Laloui, L. 2015. Energy and  
537 geotechnical behaviour of energy piles for different design solutions. *Computers and  
538 Geotechnics*, **86** (1): 199–213. <https://doi.org/10.1016/j.applthermaleng.2015.04.050>.
- 539 Bodas Freitas, T., Cruz Silva, F., and Bourne-Webb, P.J. 2013. The response of energy  
540 foundations under thermo-mechanical loading. In *Proceedings of 18th international  
541 conference on soil mechanics and geotechnical engineering*, **4**: 3347-3350. Paris,  
542 France: Comité Français de Mécanique des Sols et de Géotechnique.
- 543 Bourne-Webb, P.J., B. Amatya, K. Soga, T. Amis, C. Davidson, and P. Payne. 2009. Energy  
544 pile test at Lambeth College, London: Geotechnical and thermodynamic aspects of pile  
545 response to heat cycles. *Géotechnique*, **59**(3): 237–248.  
546 <https://doi.org/10.1680/geot.2009.59.3.237>.
- 547 Bourne-Webb, P.J., Bodas Freitas, T.M., and Freitas Assunção, R. M. 2015. Soil–pile thermal  
548 interactions in energy foundations. *Géotechnique*, **66**(2): 167-171.  
549 <https://doi.org/10.1680/jgeot.15.T.017>.
- 550 Bowles, Joseph E. 1968. *Foundation analysis and design*. New York: McGraw-Hill
- 551 Caulk, R., Ghazanfari, E., and McCartney, J.S. 2016. Parameterization of a calibrated  
552 geothermal energy pile model. *Geomechanics for Energy and the Environment*, **5**: 1-  
553 15. <https://doi.org/10.1016/j.gete.2015.11.001>.
- 554 Di Donna, A., Rotta Loria, A.F., and Laloui, L. 2016. Numerical study of the response of a  
555 group of energy piles under different combinations of thermo-mechanical loads.

- 556 Computers and Geotechnics, **72**: 126-142.  
557 <https://doi.org/10.1016/j.compgeo.2015.11.010>.
- 558 Elzeiny, R., Suleiman, M. T., Xiao, S., Abu Qamar, M. A., and Al-Khawaja, M. (2020).  
559 Laboratory-Scale Pull-Out Tests on a Geothermal Energy Pile in Dry Sand Subjected  
560 to Heating Cycles. Canadian Geotechnical Journal, (ja). [https://doi.org/10.1139/cgj-](https://doi.org/10.1139/cgj-2019-0143)  
561 [2019-0143](https://doi.org/10.1139/cgj-2019-0143).
- 562 Faizal, M., Bouazza, A., and Singh, R. M. 2016. An experimental investigation of the influence  
563 of intermittent and continuous operating modes on the thermal behaviour of a full scale  
564 geothermal energy pile. Geomechanics for Energy and the Environment, **8**: 8-29.  
565 <https://doi.org/10.1016/j.gete.2016.08.001>.
- 566 Faizal, M., Bouazza, A., Haberfield, C., and McCartney J.S. 2018. Axial and radial thermal  
567 responses of a field-scale energy pile under monotonic and cyclic temperature changes.  
568 Journal of Geotechnical and Geoenvironmental Engineering, **144**(10): 04018072.  
569 <https://doi.org/10.1139/cgj-2018-0246>.
- 570 Faizal, M., Bouazza, A., McCartney, J.S., and Haberfield, C. 2019a. Axial and radial thermal  
571 responses of an energy pile under a 6-storey residential building. Canadian  
572 Geotechnical Journal, **56**(7): 1019–1033. [https://doi.org/10.1061/\(ASCE\)GT.1943-](https://doi.org/10.1061/(ASCE)GT.1943-5606.0001952)  
573 [5606.0001952](https://doi.org/10.1061/(ASCE)GT.1943-5606.0001952).
- 574 Faizal, M., Bouazza, A., McCartney, J.S. and Haberfield, C. 2019b. Effects of cyclic  
575 temperature variations on the thermal response of an energy pile under a residential  
576 building. Journal of Geotechnical and Geoenvironmental Engineering **145** (10):  
577 04019066. [https://doi.org/10.1061/\(ASCE\)GT.1943-5606.0002147](https://doi.org/10.1061/(ASCE)GT.1943-5606.0002147)
- 578 Gawecka, K.A., Taborda, D.M.G., Potts, D.M., Cui, W., Zdravković, L., and Kasri, M.S.H.  
579 2017. Numerical modelling of thermo-active piles in London Clay. Proceedings of the  
580 Institution of Civil Engineers - Geotechnical Engineering, **170**(3): 201-219.

- 581 Gnielinski, V. 1975. New equations for heat and mass transfer in the turbulent flow in pipes  
582 and channels. NASA STI/recon technical report A, **75**: 8-16.
- 583 Guo, Y., Zhang, G., and Liu, S. 2018. Investigation on the thermal response of full-scale PHC  
584 energy pile and ground temperature in multi-layer strata. Applied Thermal  
585 Engineering, **143**: 836–848. <https://doi.org/10.1016/j.applthermaleng.2018.08.005>.
- 586 Haaland, S.E. 1983. Simple and explicit formulas for the friction factor in turbulent pipe flow.  
587 Journal of Fluids Engineering, **105**(1): 89-90.
- 588 Hamada, Y., Saitoh, H., Nakamura, M., Kubota, H., and Ochifuji, K. 2007. Field performance  
589 of an energy pile system for space heating. Energy and Buildings, **39**(5): 517-524.  
590 <https://doi.org/10.1016/j.enbuild.2006.09.006>.
- 591 Jeong, S., Lim, H., Lee, J.K., and Kim, J. 2014. Thermally induced mechanical response of  
592 energy piles in axially loaded pile groups. Applied Thermal Engineering, **71**(1): 608-  
593 615. <https://doi.org/10.1016/j.applthermaleng.2014.07.007>.
- 594 Khosravi, A., Moradshahi, A., McCartney, J.S., and Kabiri, M. 2016. Numerical analysis of  
595 energy piles under different boundary conditions and thermal loading cycles. E3S Web  
596 Conference, **9**: 05005. EDP Sciences.
- 597 Laloui, L., Nuth, M., and Vulliet, L. 2006. Experimental and numerical investigations of the  
598 behaviour of a heat exchanger pile. International Journal for Numerical and Analytical  
599 Methods in Geomechanics, **30**(8): 763-781. <https://doi.org/10.1002/nag.499>.
- 600 McCartney, J.S. and K.D. Murphy 2012. Strain distributions in full-scale energy foundations.  
601 DFI Journal - The Journal of the Deep Foundations Institute, **6**(2): 26-38.  
602 <https://doi.org/10.1179/dfi.2012.008>.
- 603 McCartney, J.S., and Murphy, K.D. 2017. Investigation of potential dragdown/uplift effects on  
604 energy piles. Geomechanics for Energy and the Environment, **10**: 21-28.  
605 <https://doi.org/10.1016/j.gete.2017.03.001>.

- 606 Mimouni, T., and Laloui, L. 2015. Behaviour of a group of energy piles. Canadian  
607 Geotechnical Journal, **52**(12): 1913-1929. <https://doi.org/10.1139/cgj-2014-0403>.
- 608 Mitchell, J.K. and Soga, K. 2005. Fundamentals of soil behavior, 3<sup>rd</sup> edition. Wiley, New Jersey.
- 609 Murphy, K.D., and McCartney, J.S. 2014. Seasonal response of energy foundations during  
610 building operation. Geotechnical and Geological Engineering, **33**(2): 343-356.  
611 <https://doi.org/10.1007/s10706-014-9802-3>.
- 612 Murphy, K.D., McCartney, J.S., and Henry, K. S. 2015. Evaluation of thermo-mechanical and  
613 thermal behavior of full-scale energy foundations. Acta Geotechnica, **10**(2): 179-195.  
614 <https://doi.org/10.1007/s11440-013-0298-4>.
- 615 Olgun, C., Ozudogru, T., and Arson. 2014. Thermo-mechanical radial expansion of heat  
616 exchanger piles and possible effects on contact pressures at pile–soil interface.  
617 Géotechnique Letters, **4**(3): 170-178. <https://doi.org/10.1680/geolett.14.00018>.
- 618 Ozudogru, T.Y., Olgun, C.G., and Arson, C.F. 2015. Analysis of friction induced thermo-  
619 mechanical stresses on a heat exchanger pile in isothermal soil. Geotechnical and  
620 Geological Engineering, **33**(2): 357-371. <https://doi.org/10.1007/s10706-014-9821-0>.
- 621 Peng, H.F., Kong, G.Q., Liu, H.L., Abuel-Naga, H., and Hao, Y. H. 2018. Thermo-mechanical  
622 behaviour of floating energy pile groups in sand. Journal of Zhejiang University-  
623 SCIENCE A, **19**(8): 638-649. <https://doi.org/10.1631/jzus.A1700460>.
- 624 Ravera, E., Sutman, M. and Laloui, L., 2019. Analysis of the interaction factor method for  
625 energy pile groups with slab. Computers and Geotechnics, p.103294.  
626 <https://doi.org/10.1016/j.compgeo.2019.103294>.
- 627 Rotta Loria, A.F. and Laloui, L. 2016. The interaction factor method for energy pile groups.  
628 Computers and Geotechnics, **80**: 121-137.  
629 <https://doi.org/10.1016/j.compgeo.2016.07.002>.

- 630 Rotta Loria, A.F. and Laloui, L. 2017a. The equivalent pier method for energy pile groups.  
631 *Géotechnique*, **67**(8): 691–702. <https://doi.org/10.1680/jgeot.16.P.139>.
- 632 Rotta Loria, A.F. and Laloui, L. 2017b. Thermally induced group effects among energy piles.  
633 *Géotechnique*, **67**(5): 374-393. <https://doi.org/10.1680/jgeot.16.P.039>.
- 634 Rotta Loria, A. F. and Laloui, L. 2018. Group action effects caused by various operating energy  
635 piles. *Géotechnique*, **68**(9): 834-841. <https://doi.org/10.1680/jgeot.17.P.213>.
- 636 Saggiu, R., and Chakraborty, T. 2016. Thermo-mechanical response of geothermal energy pile  
637 groups in sand. *International Journal of Geomechanics*, **16**(4): 04015100.  
638 [https://doi.org/10.1061/\(ASCE\)GM.1943-5622.0000567](https://doi.org/10.1061/(ASCE)GM.1943-5622.0000567).
- 639 Salciarini, D., Ronchi, F., Cattoni, E., and Tamagnini, C. 2015. Thermo-mechanical effects  
640 induced by energy piles operation in a small piled raft. *International Journal of*  
641 *Geomechanics*, **15**(2): 04014042. [https://doi.org/10.1061/\(ASCE\)GM.1943-](https://doi.org/10.1061/(ASCE)GM.1943-5622.0000375)  
642 [5622.0000375](https://doi.org/10.1061/(ASCE)GM.1943-5622.0000375).
- 643 Sani, A.K., Singh, R.M., Tsuha, C.de H.C., and Cavarretta, I. (2019). Pipe–pipe thermal  
644 interaction in a geothermal energy pile. *Geothermics*, **81**: 209–223.  
645 <https://doi.org/10.1016/j.geothermics.2019.05.004>.
- 646 Singh, R., Bouazza, A., and Wang, B. 2015. Near-field ground thermal response to heating of  
647 a geothermal energy pile: Observations from a field test. *Soils and Foundations*, **55**(6):  
648 1412-1426. <https://doi.org/10.1016/j.sandf.2015.10.007>.
- 649 Stewart, M. A., and McCartney, J. S. 2014. Centrifuge modeling of soil-structure interaction  
650 in energy foundations. *Journal of Geotechnical and Geoenvironmental Engineering*,  
651 **140**(4): 04013044-1-11. [https://doi.org/10.1061/\(ASCE\)GT.1943-5606.0001061](https://doi.org/10.1061/(ASCE)GT.1943-5606.0001061).
- 652 Suryatriyastuti, M.E., Mroueh, H., and Burlon, S. 2012. Understanding the temperature-  
653 induced mechanical behaviour of energy pile foundations. *Renewable and Sustainable*  
654 *Energy Reviews*, **16**(5): 3344-3354. <https://doi.org/10.1016/j.rser.2012.02.062>.

- 655 Suryatriyastuti, M.E., Burlon, S., and Mroueh, H. 2016. On the understanding of cyclic  
656 interaction mechanisms in an energy pile group. *International Journal for Numerical*  
657 *and Analytical Methods in Geomechanics*, **40**(1): 3-24.  
658 <https://doi.org/10.1002/nag.2382>.
- 659 Sutman, M., Brettmann, T. and Olgun, C.G., 2019. Full-scale in-situ tests on energy piles: Head  
660 and base-restraining effects on the structural behaviour of three energy  
661 piles. *Geomechanics for Energy and the Environment*, **18**: 56-68.  
662 <https://doi.org/10.1016/j.gete.2018.08.002>.
- 663 You, S., Cheng, X., Guo, H., and Yao, Z. 2014. In-situ experimental study of heat exchange  
664 capacity of CFG pile geothermal exchangers. *Energy and Buildings*, **79**: 23-31.  
665 <https://doi.org/10.1016/j.enbuild.2014.04.021>.
- 666 Wang, B., Bouazza, A., Singh, R.M., Haberfield, C., Barry-Macaulay, D., and Baycan, S., 2015.  
667 Posttemperature effects on shaft capacity of a full-scale geothermal energy pile. *Journal*  
668 *of Geotechnical and Geoenvironmental Engineering*, **141**(4): 04014125.  
669 [https://doi.org/10.1061/\(ASCE\)GT.1943-5606.0001266](https://doi.org/10.1061/(ASCE)GT.1943-5606.0001266).
- 670 Wu, D., Liu, H.L., Kong, G.Q., Ng, C.W.W., and Cheng, X.H. 2018. Displacement response  
671 of an energy pile in saturated clay. *Proceedings of the Institution of Civil Engineers-*  
672 *Geotechnical Engineering*, **171**(4): 285-294. <https://doi.org/10.1680/jgeen.17.00152>.
- 673 Wu, D., Liu, H., Kong, G., and Ng, C.W.W. (2020). Interactions of an energy pile with several  
674 traditional piles in a row. *Journal of Geotechnical and Geoenvironmental*  
675 *Engineering*, **146**(4). [https://doi.org/10.1061/\(ASCE\)GT.1943-5606.0002224](https://doi.org/10.1061/(ASCE)GT.1943-5606.0002224).
- 676  
677  
678  
679  
680  
681

682

683

684 **LIST OF FIGURE CAPTIONS**

685 **Figure 1.** Field scale energy piles instrumentation and WVSGs locations (after Faizal et al.  
686 2019).

687 **Figure 2.** Inlet water temperatures during the three experiments.

688 **Figure 3.** Finite element mesh of the numerical model (a) 3D view; (b) plan view; (c) side view  
689 of energy pile and heat exchanger loops; (d) plan view of energy pile and heat exchanger loops.

690 **Figure 4.** Experimental and numerical profiles of EP1 (a) temperatures from radial WVSGs;  
691 (b) temperatures from axial WVSGs; (c) radial thermal strains; (d) axial thermal strains; (e)  
692 radial thermal stresses; (f) axial thermal stresses.

693 **Figure 5.** Experimental and numerical soil temperature distributions between the two energy  
694 piles: (a) versus depth; (b) versus radial distance at a depth of 5 m.

695 **Figure 6.** Ambient and inlet fluid temperatures used in the parametric analyses: (a) ambient  
696 atmospheric temperature; (b) inlet fluid temperature.

697 **Figure 7.** Effect of varying soil thermal conductivity on (a) EP1 temperature; (b) ground  
698 temperature.

699 **Figure 8.** Axial thermal responses of EP1 from the parametric evaluation: (a) strains when  
700 varying  $E_{soil}$ ; (b) stresses when varying  $E_{soil}$ ; (c) strains when varying  $\lambda_{soil}$ ; (d) stresses when  
701 varying  $\lambda_{soil}$ ; (e) strains when varying  $\alpha_{soil}$ ; (f) stresses when varying  $\alpha_{soil}$ .

702 **Figure 9.** Radial thermal responses of EP1 from the parametric evaluation: (a) strains when  
703 varying  $E_{soil}$ ; (b) stresses when varying  $E_{soil}$ ; (c) strains when varying  $\lambda_{soil}$ ; (d) stresses when  
704 varying  $\lambda_{soil}$ ; (e) strains when varying  $\alpha_{soil}$ ; (f) stresses when varying  $\alpha_{soil}$ .

705 **Figure 10.** Radial ( $\delta_{TR}$ ) and axial ( $\delta_{TA}$ ) thermal displacements of EP1 from the parametric  
706 evaluation: (a)  $\delta_{TR}$  when varying  $E_{soil}$ ; (b)  $\delta_{TA}$  when varying  $E_{soil}$ ; (c)  $\delta_{TR}$  when varying  $\lambda_{soil}$ ; (d)  
707  $\delta_{TA}$  when varying  $\lambda_{soil}$ ; (e)  $\delta_{TR}$  when varying  $\alpha_{soil}$ ; (f)  $\delta_{TA}$  when varying  $\alpha_{soil}$ .

## 708 LIST OF TABLES

709 **Table 1.** Material properties for numerical simulations calibrated against field test  
710 measurements

711

712

713

714

715

716

717

718

719

720

721

722

723

724

725

726

727

728

729

730

731

732

733

734

735

736

737

738

739

740



741  
742  
743  
744  
745  
746

**Table 1.** Material properties for numerical simulations calibrated against field test measurements

<b>Material</b>	Depth $z$ [m]	Elastic modulus $E$ [MPa]	Poisson's ratio $\nu$ [—]	Porosity $n$ [—]	Total density $\rho$ [kg/m <sup>3</sup> ]	Specific heat $C_p$ [J/kgK]	Thermal Conductivity $\lambda$ [W/(mK)]	Coef. Therm. Exp. $\alpha$ [ $\mu\epsilon/^\circ\text{C}$ ]
Fill	0.0- 0.5	15	0.3	0.35	1750	800	1.1	10
Sand	0.5- 3.5	500	0.25	0.33	1800	840	1.7	10
Sandy clay	3.5- 6.0	75	0.30	0.33	1950	810	2.0	10
Sand	6.0- 12.5	120	0.25	0.30	2200	850	2.3	10
Pile	—	35000	0.22	—	2500	810	1.5	13
Slab	—	35000	0.20	—	2500	850	1.5	13
HDPE pipes	—	—	—	—	—	—	0.4	—

747  
748  
749  
750  
751  
752  
753  
754  
755

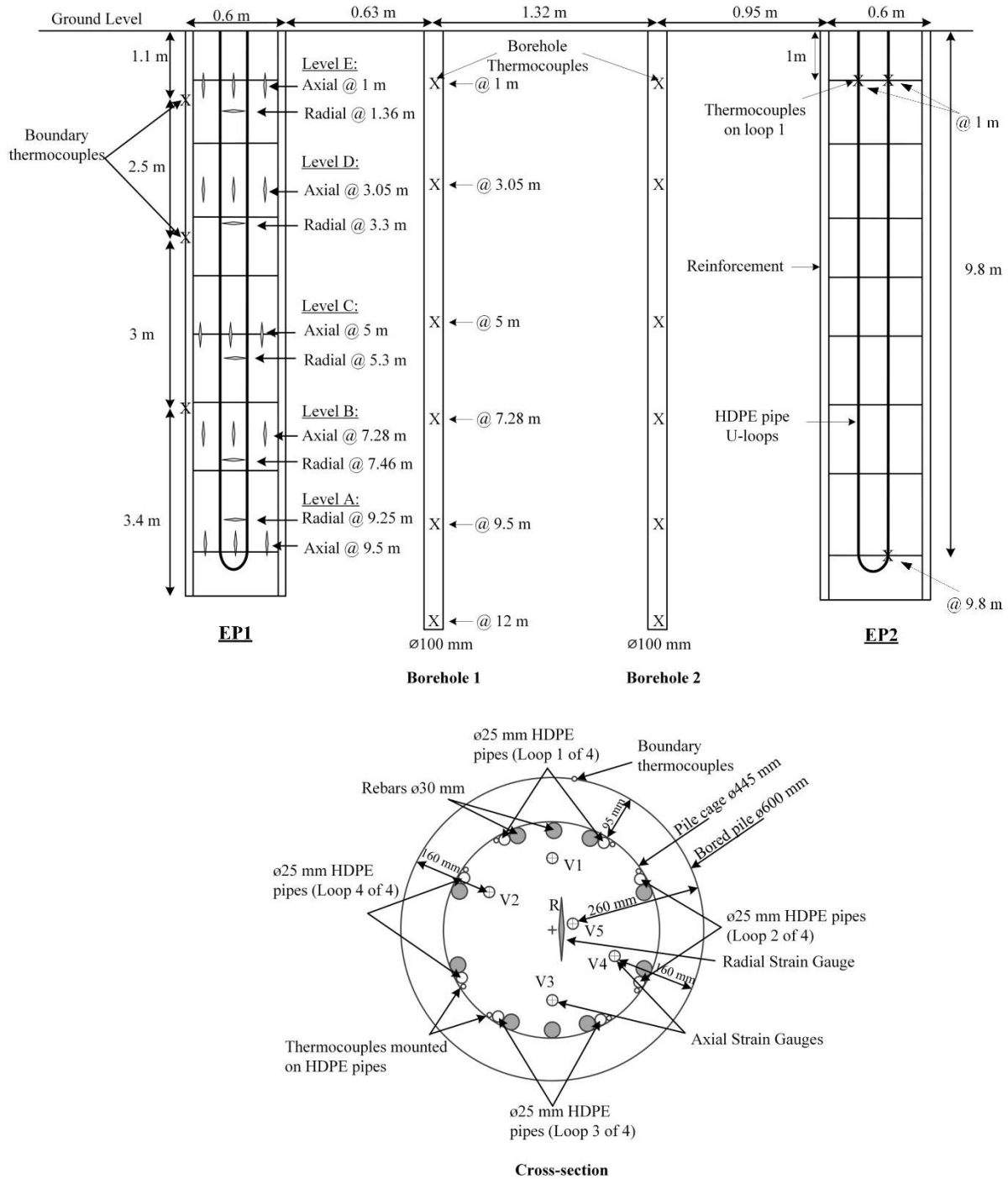


**Figure 1.** Field scale energy piles instrumentation and WVSGs locations (after Faizal et al. 2019).

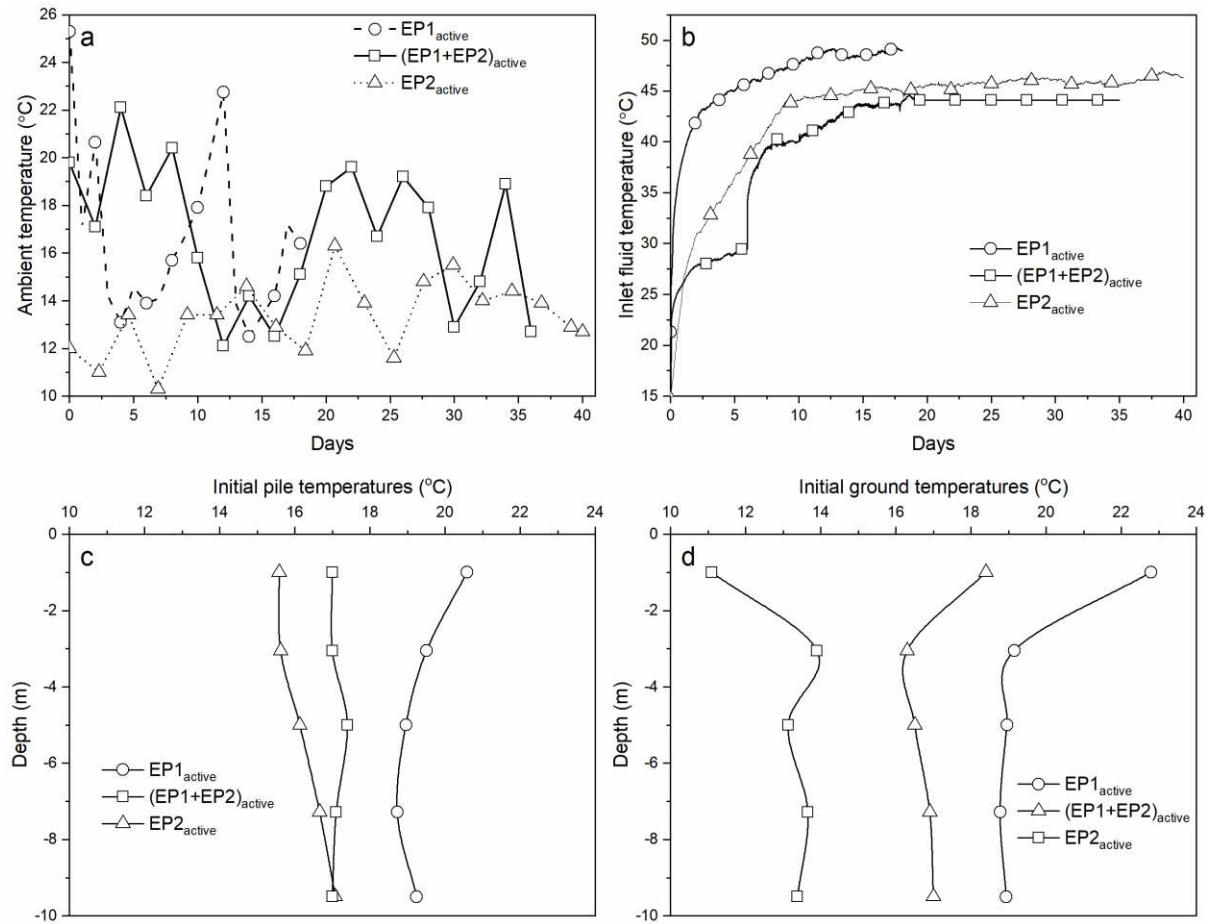


**Figure 2.** Ambient, inlet fluid temperature, and initial pile and ground during three experiments: (a) ambient atmospheric temperature; (b) inlet fluid temperature; (c) initial pile temperatures; and (d) initial ground temperatures.

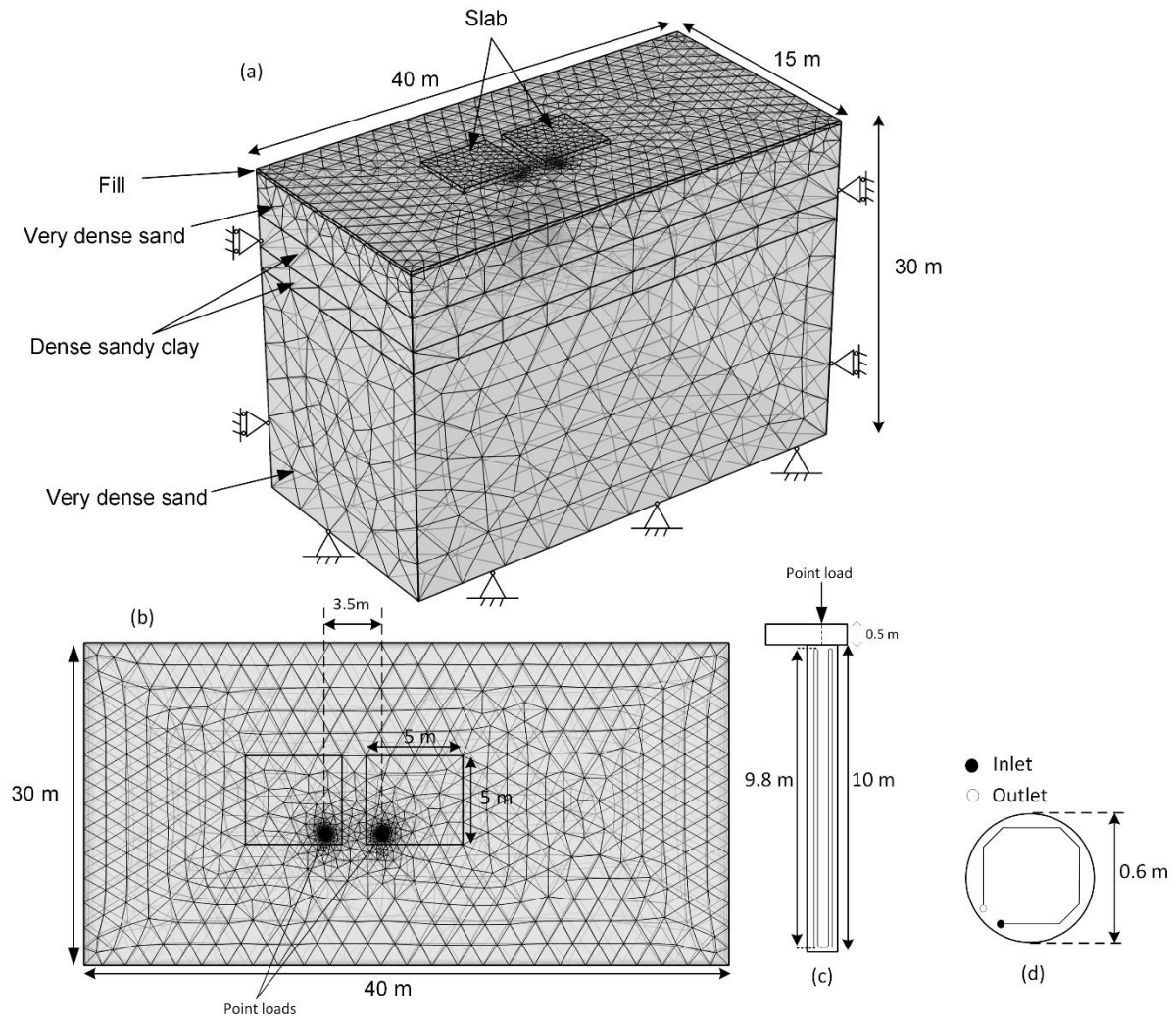


**Figure 3.** Finite element mesh of the numerical model (a) 3D view; (b) plan view; (c) side view of energy pile and heat exchanger loops; (d) plan view of energy pile and heat exchanger loops.

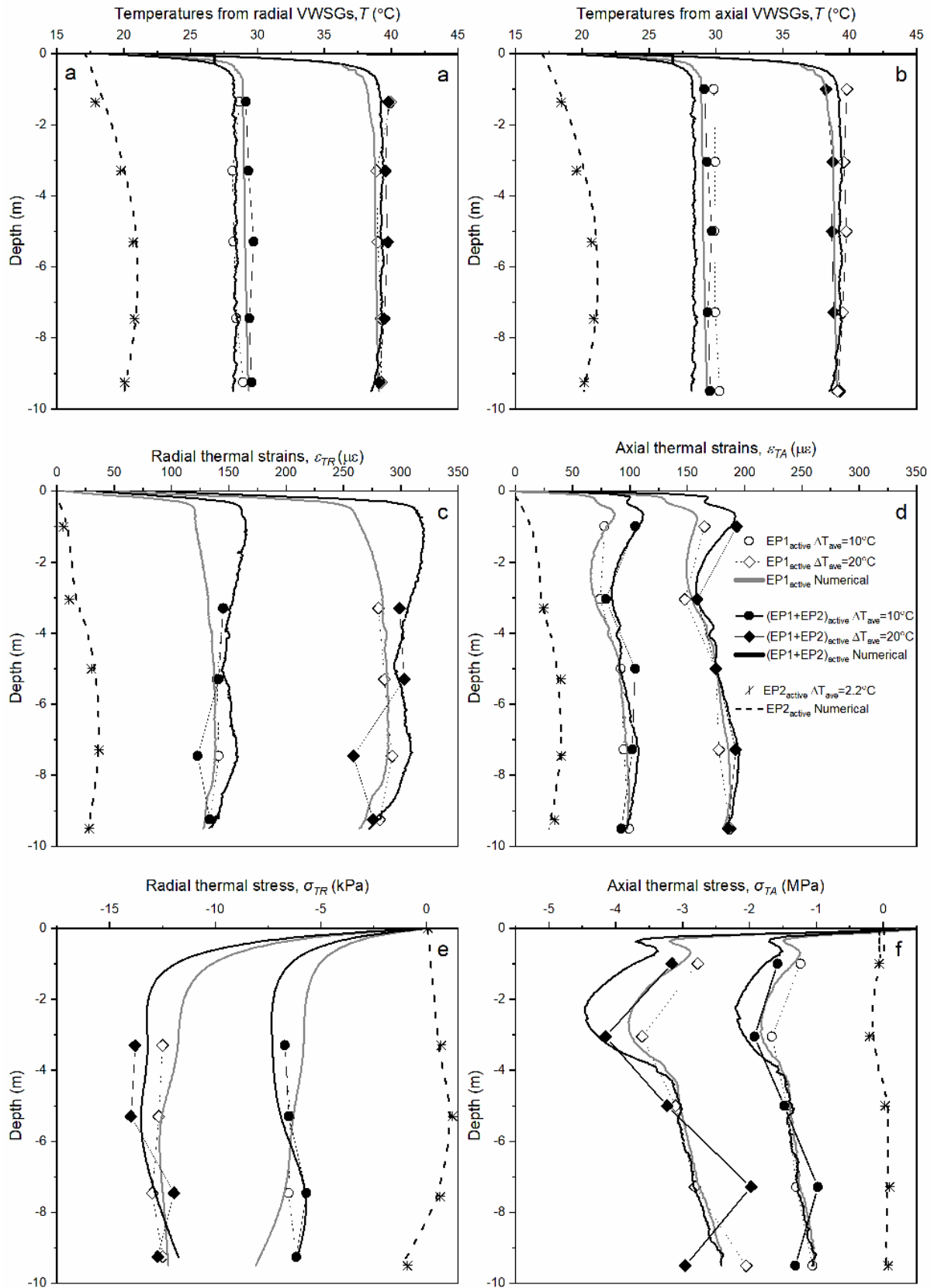


**Figure 4.** Experimental and numerical profiles of EP1 (a) temperatures from radial VWSGs; (b) temperatures from axial VWSGs; (c) radial thermal strains; (d) axial thermal strains; (e) radial thermal stresses; (f) axial thermal stresses.

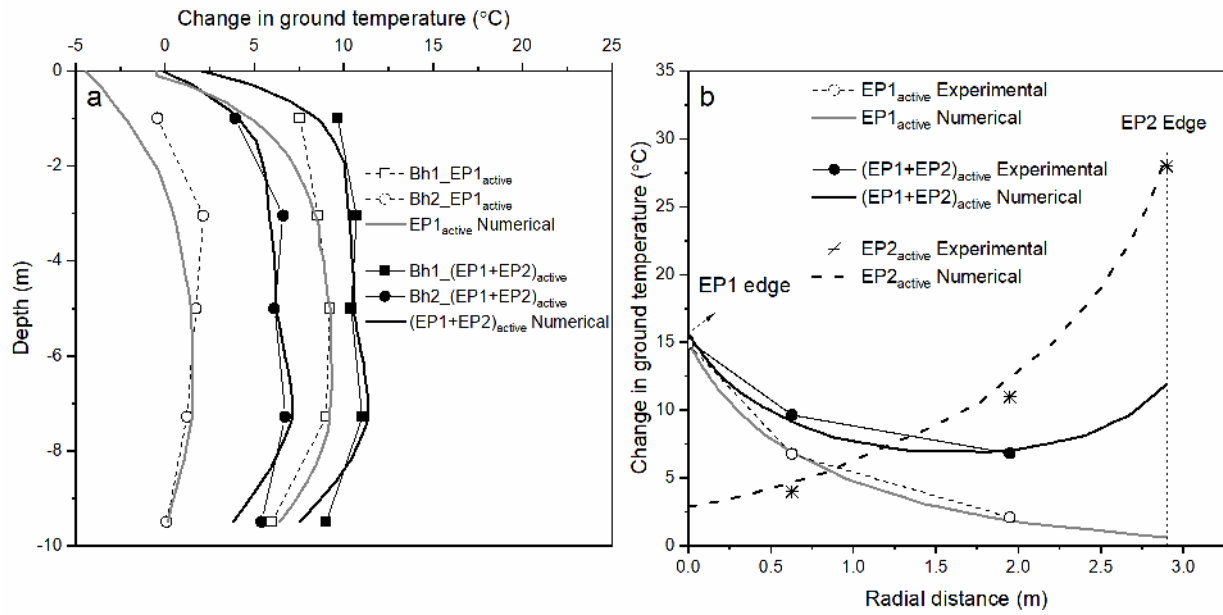


**Figure 5.** Experimental and numerical soil temperature distributions between the two energy piles: (a) versus depth; (b) versus radial distance at a depth of 5 m.

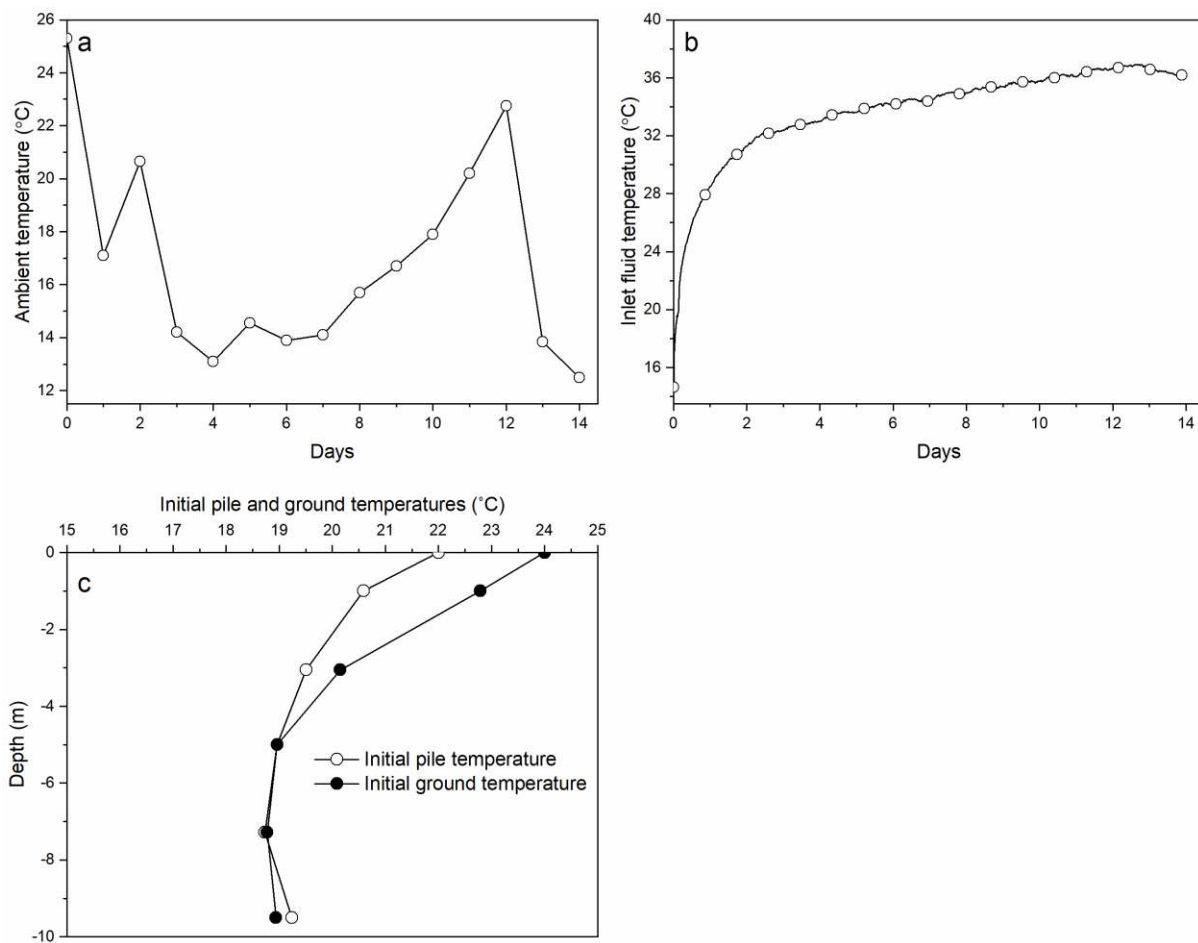


**Figure 6.** Ambient, inlet fluid temperature, and initial pile and ground temperature used in the parametric analyses: (a) ambient atmospheric temperature; (b) inlet fluid temperature; and (c) initial pile and ground temperatures.

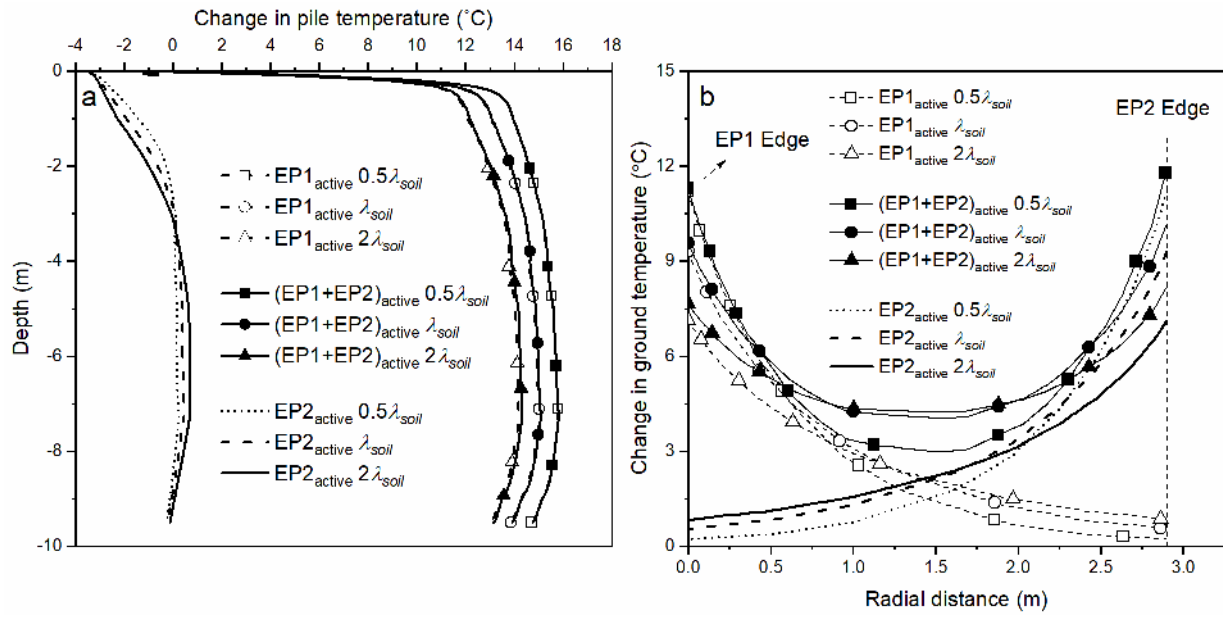


**Figure 7.** Effect of varying soil thermal conductivity on (a) EP1 temperature; (b) ground temperature.



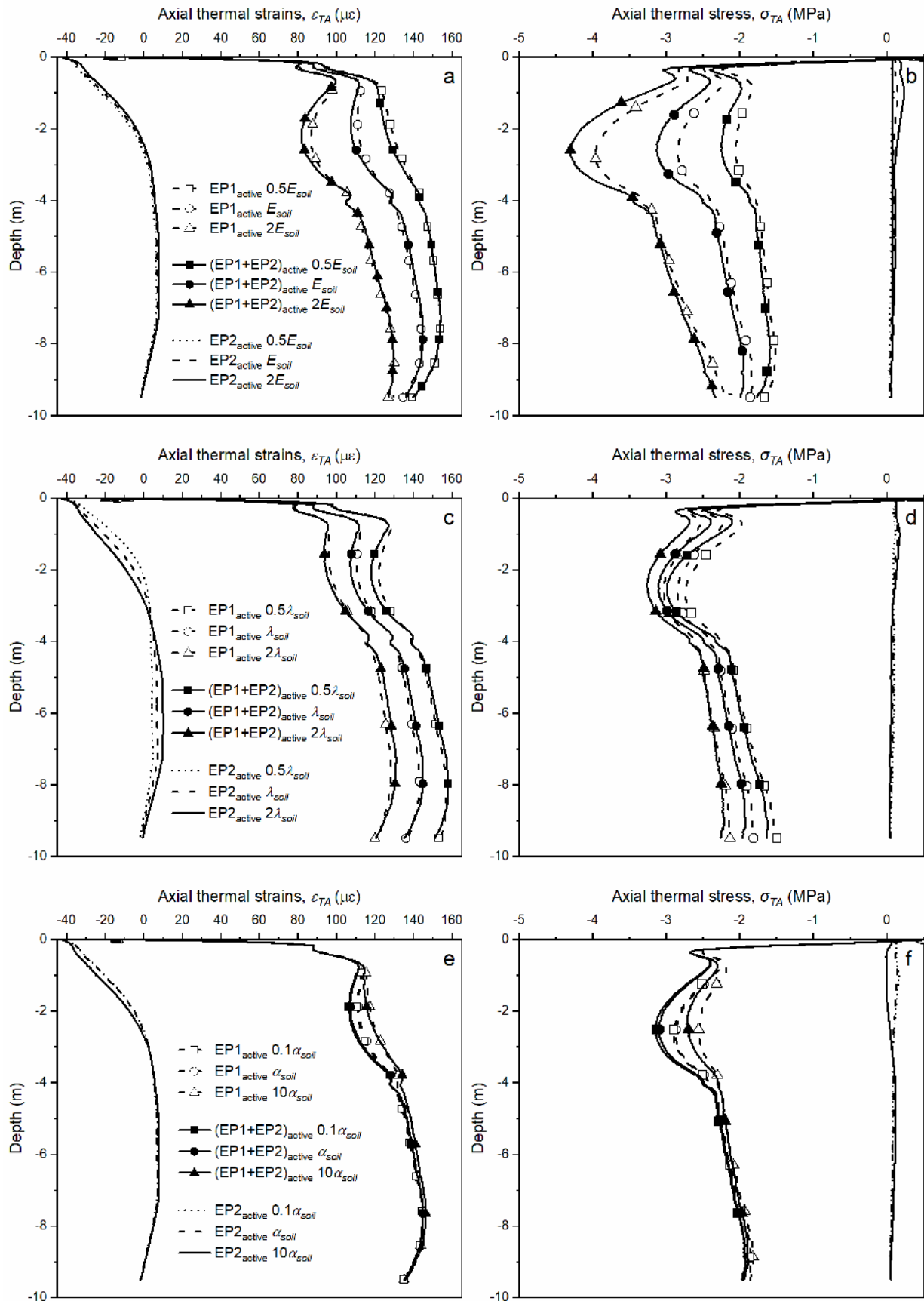


**Figure 8.** Axial thermal responses of EP1 from the parametric evaluation: (a) strains when varying  $E_{soil}$ ; (b) stresses when varying  $E_{soil}$ ; (c) strains when varying  $\lambda_{soil}$ ; (d) stresses when varying  $\lambda_{soil}$ ; (e) strains when varying  $\alpha_{soil}$ , (f) stresses when varying  $\alpha_{soil}$ .

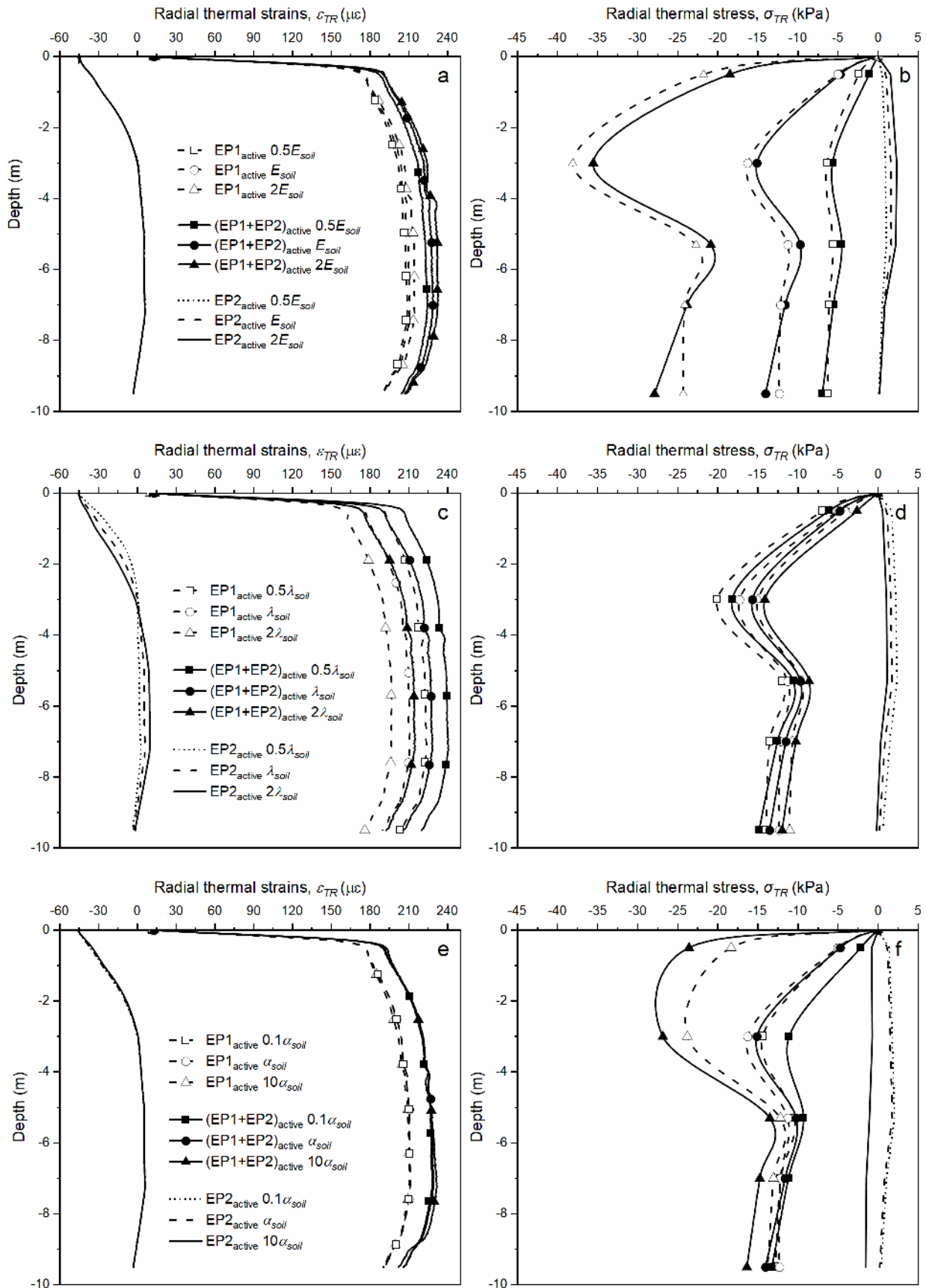


**Figure 9.** Radial thermal responses of EP1 from the parametric evaluation: (a) strains when varying  $E_{soil}$ ; (b) stresses when varying  $E_{soil}$ ; (c) strains when varying  $\lambda_{soil}$ ; (d) stresses when varying  $\lambda_{soil}$ ; (e) strains when varying  $\alpha_{soil}$ , (f) stresses when varying  $\alpha_{soil}$ .

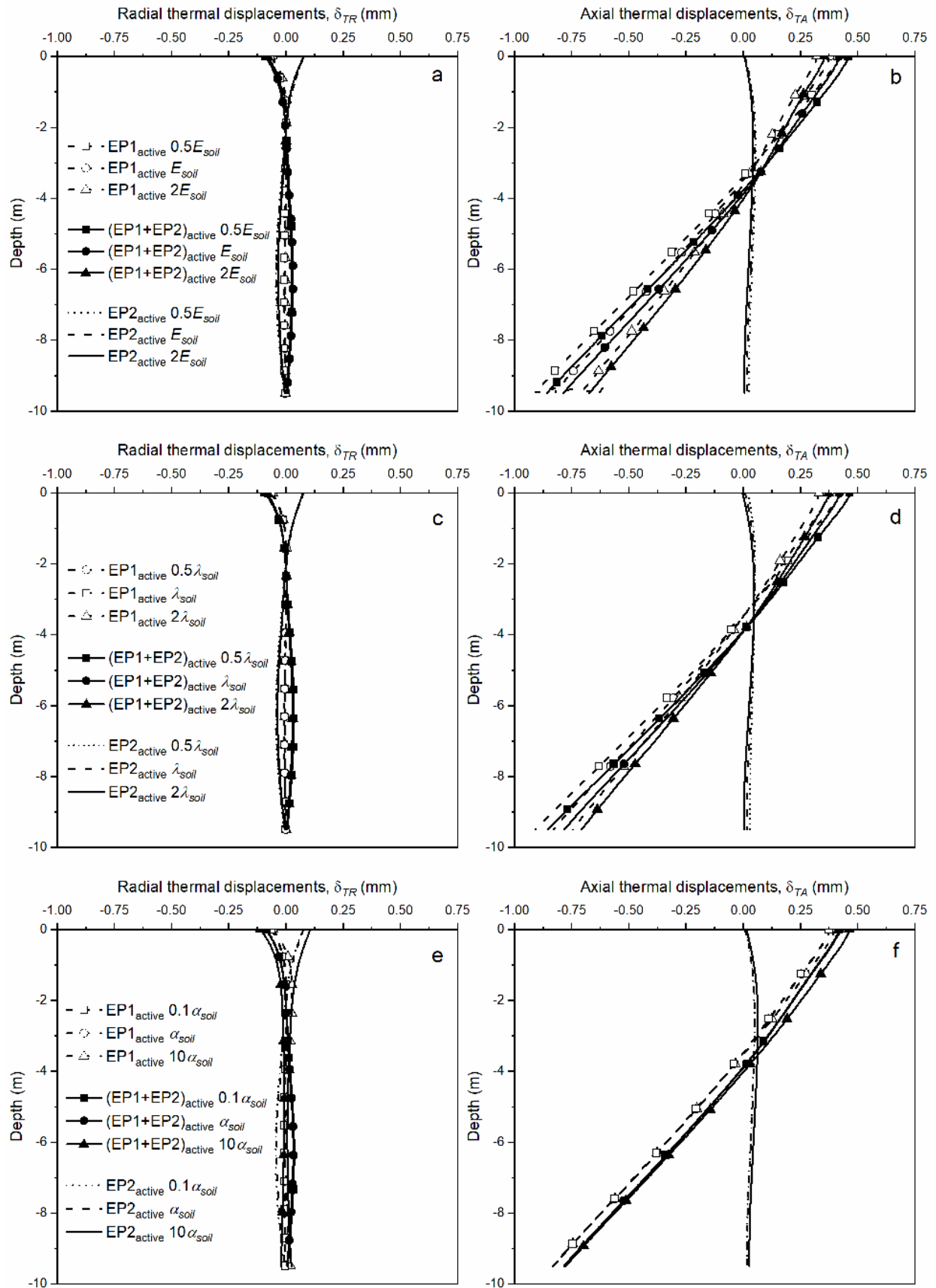


**Figure 10.** Radial ( $\delta_{TR}$ ) and axial ( $\delta_{TA}$ ) thermal displacements of EP1 from the parametric evaluation: (a)  $\delta_{TR}$  when varying  $E_{soil}$ ; (b)  $\delta_{TA}$  when varying  $E_{soil}$ ; (c)  $\delta_{TR}$  when varying  $\lambda_{soil}$ ; (d)  $\delta_{TA}$  when varying  $\lambda_{soil}$ ; (e)  $\delta_{TR}$  when varying  $\alpha_{soil}$ ; (f)  $\delta_{TA}$  when varying  $\alpha_{soil}$ .